https://doi.org/10.5194/egusphere-2023-2293
Preprint. Discussion started: 26 October 2023

Incorporating Oxygen Isotopes of Oxidized Reactive Nitrogen in the Regional Atmospheric Chemistry Mechanism, Version 2 (ICOIN-RACM2)

Wendell W. Walters[1,2,3], Masayuki Takeuchi[4], Nga L. Ng[4,5,6], and Meredith G. Hastings[2,3]

[1]Department of Chemistry and Biochemistry, University of South Carolina, 631 Sumter St, Columbia, SC 29208
[2]Institute at Brown for Environment and Society, Brown University, 85 Waterman St, Providence, RI 02912
[3]Department of Earth, Environmental, and Planetary Sciences, Brown University, 324 Brook Street, Box 1846, Providence, RI 02912
[4]School of Civil and Environmental Engineering, Georgia Institute of Technology, 311 Ferst Drive NW, Atlanta, GA 30332
[5]School of Chemical and Biomolecular Engineering, Georgia Institute of Technology, 311 Ferst Drive NW, Atlanta, GA 30332
[6]School of Earth and Atmospheric Sciences, Georgia Institute of Technology, 311 Ferst Drive NW, Atlanta, GA 30332

Correspondence: Wendell W. Walters (wendellw@mailbox.sc.edu)

Abstract. The oxygen-stable isotope mass-independent composition ($\Delta(^{17}O) = \delta(^{17}O) - 0.52\times\delta(^{18}O)$) has proven to be a robust tool for probing photochemical cycling and atmospheric formation pathways of oxidized reactive nitrogen (NO_y). Several studies have developed modeling techniques to implicitly model $\Delta(^{17}O)$ based on numerous assumptions that may not always be valid. Thus, these models may be oversimplified and limit our ability to compare model $\Delta(^{17}O)$ values of NO_y with observations. In this work, we introduce a novel method for explicit tracking of O_3 transfer and propagation into NO_y and odd oxygen (O_x), integrated into the Regional Atmospheric Chemistry Mechanism, version 2 (RACM2). Termed ICOIN-RACM2 (InCorporating Oxygen Isotopes of NO_y in RACM2), this new model includes the addition of 55 new species and 727 replicate reactions to represent the oxygen isotopologues of NO_y and O_x. Employing this mechanism within a box model, we simulate $\Delta(^{17}O)$ for various NO_y and O_x molecules for chamber experiments with varying initial nitrogen oxides (NO_x = NO + NO_2) and α-pinene conditions, revealing response shifts in $\Delta(^{17}O)$ linked to distinct oxidant conditions. Furthermore, diel cycles are simulated under two summertime scenarios, representative of an urban and rural site, revealing pronounced $\Delta(^{17}O)$ diurnal patterns for several NO_y components and substantial $\Delta(^{17}O)$ differences associated with pollution levels (urban vs. rural). Overall, the proposed mechanism offers the potential to assess NO_y oxidation chemistry in chamber studies and air quality campaigns through $\Delta(^{17}O)$ model comparisons against observations. The integration of this mechanism into a 3-D atmospheric chemistry transport model is expected to notably enhance our capacity to model and anticipate $\Delta(^{17}O)$ across landscapes, consequently refining model representations of atmospheric chemistry and tropospheric oxidation capacity.

1 Introduction

Nitrogen oxides (NO_x = NO + NO_2) are essential trace gases primarily released through human activities, carrying significant implications for air quality, nutrient deposition, and the climate system (Galloway et al., 2004; Pinder et al., 2012). NO_x di-

https://doi.org/10.5194/egusphere-2023-2293
Preprint. Discussion started: 26 October 2023

rectly modulates atmospheric oxidation processes, consequently impacting the concentrations of various trace gases, including greenhouse gases (Prinn, 2003). Ultimately, NO_x is removed from the atmosphere as atmospheric nitrate. This global process is dominated by the formation of inorganic nitrate, encompassing nitric acid (HNO_3) and particulate nitrate (pNO_3) (Alexander et al., 2019), although the generation of organic nitrates ($RONO_2$) might be significant in remote and rural areas (Browne and Cohen, 2012). However, both pNO_3 and $RONO_2$ may not be a terminal sink for NO_x due to the potential for renoxification from photolysis (Wang et al., 2023; Gen et al., 2022). Uncertainties surrounding the rate of NO_x oxidation to atmospheric nitrate constitute a substantial source of ambiguity in models, influencing ozone (O_3) and hydroxyl radical (OH) formation, with important implications for greenhouse gas removal rates (Newsome and Evans, 2017).

The oxygen mass-independent stable isotope composition ($\Delta(^{17}O) = \delta(^{17}O) - 0.52 \times \delta(^{18}O)$) has emerged as a potent tool for evaluating the photochemical cycling and oxidation chemistry of NO_x and its oxidized products (NO_y = (NO_x + HNO_3 + $RONO_2$ + nitrous acid (HONO) + peroxyacetyl nitrate (PAN) + etc) (Alexander et al., 2019, 2009; Hastings et al., 2003; Michalski et al., 2003; Morin et al., 2011; Walters et al., 2019). This is facilitated by the distinctive $\Delta(^{17}O)$ in atmospheric ozone associated with unconventional isotope effects during its formation (Gao and Marcus, 2001). Tropospheric O_3, for instance, exhibits a "bulk" $\Delta(^{17}O)$ value near 26 ‰ (Johnston and Thiemens, 1997) and a value of (39.3 ± 2.3 ‰) associated with the terminal O-atoms of O_3 (termed $\Delta(^{17}O, O_3^{term})$) (Vicars and Savarino, 2014). The terminal O-atoms of O_3 are preferentially transferred to reaction products (Savarino et al., 2008). In contrast, most other oxygen-bearing atmospheric molecules, such as oxygen (O_2), water (H_2O), and peroxy radicals (RO_2 or HO_2), possess (or expected to possess) $\Delta(^{17}O)$ values near 0 ‰ (Lyons, 2001). These large $\Delta(^{17}O)$ differences enable the quantitative tracking of the influence of O_3 in NO_x oxidation chemistry.

Past observations of $\Delta(^{17}O)$ in atmospheric nitrate, which includes HNO_3, pNO_3, and wet-deposited nitrate ($NO_3^-{}_{(aq)}$), have generally shown marked seasonal variations, reflecting shifts between O_3 and HO_x chemical regimes influencing NO_x photochemical cycling and atmospheric nitrate production (Kim et al., 2023; Michalski et al., 2012, 2003). However, harnessing the full diagnostic potential of $\Delta(^{17}O)$ observations necessitates a model framework that can accurately assess and refine the representation of nitrate chemistry while linking it to nitrogen deposition and air quality. Several 0-D box models and a single 3-D global atmospheric chemistry model have been developed to simulate $\Delta(^{17}O)$ (Michalski et al., 2003; Morin et al., 2011; Alexander et al., 2019, 2009). These models often rely on implicit tagging of NO_2 and HNO_3 production rates, underpinned by assumptions regarding oxygen-isotope mass-balance calculations, NO_x photochemical cycling dynamics, and $\Delta(^{17}O)$ values of reactive oxygen species (O_x).

While most existing $\Delta(^{17}O)$ measurements pertain to atmospheric nitrate from deposition and filter samples, our capability to measure $\Delta(^{17}O)$ in other NO_y molecules has been rapidly expanding (Walters et al., 2018; Blum et al., 2020; Albertin et al., 2021; Blum et al., 2023; Chai and Hastings, 2018). Based on oxygen isotope mass-balance principles, substantial $\Delta(^{17}O)$ variations are anticipated among different NO_y including NO_2, HONO, peroxy nitrates (RO_2NO_2, organic nitrates ($RONO_2$), and HNO_3), contingent upon their formation pathways (Table 1). These mass-balance considerations necessitate precise knowledge of the $\Delta(^{17}O)$ values for several NO_y and O_x molecules. Conventional model approaches have assumed that $\Delta(^{17}O$, OH,

https://doi.org/10.5194/egusphere-2023-2293
Preprint. Discussion started: 26 October 2023

RO_2, HO_2) are approximately equal to 0 ‰, due to water vapor isotope exchange or transfer of O-atoms from atmospheric O_2 with a $\Delta(^{17}O, O_2, H_2O)$ near 0 ‰ (Michalski et al., 2012; Barkan and Luz, 2003). However, some of these assumptions are not valid for all relevant atmospheric conditions, such as under low relative humidity and high NO_x conditions, in which the chemical reactivity of OH could be higher than its chemical lifetime to achieve isotope equilibrium with H_2O (Michalski et al., 2012). Further, $\Delta(^{17}O, NO)$ is commonly assumed to be equal to $\Delta(^{17}O, NO_2)$ due to their rapid photochemical cycling, such that the $\Delta(^{17}O, NO, NO_2)$ values reflect the relative contributions of the oxidants involved in NO_x photochemical cycling (Alexander et al., 2019, 2009; Michalski et al., 2003; Morin et al., 2011). However, recent diel observations of $\delta(^{18}O, NO_2)$ (which tracks with $\Delta(^{17}O)$) and $\Delta(^{17}O, NO_2)$ reveal that this assumption is not universally valid due to substantial nocturnal NO emissions close to the surface, which perturb $\delta(^{18}O)$ and $\Delta(^{17}O)$ of NO_2 out of photochemical equilibrium with the atmospheric oxidants involved in the Leighton Cycle (Walters et al., 2018; Albertin et al., 2021). The nocturnal primary emissions of NO_y components including NO, NO_2, and HONO significantly impacts our ability to model $\Delta(^{17}O)$ using implicit methods in polluted regions, employing prior modeling techniques and oxygen isotope mass-balance calculations. This modeling limitation presently impedes our capacity to leverage models for comparison with $\Delta(^{17}O)$ observational constraints quantitatively to improve understanding of regional and global NO_x oxidation chemistry.

This study is dedicated to addressing uncertainties in modeling $\Delta(^{17}O)$ for various NO_y molecules. We introduce a novel gas-phase chemical mechanism, designated "InCorporating Oxygen Isotopes of NO_y in RACM2," built upon the foundation of the Regional Atmospheric Chemistry Model, Version 2 (RACM2) (Goliff et al., 2013). This innovative mechanism explicitly traces the transfer and propagation of oxygen atoms from O_3 into NO_y molecules, with important future implications for chamber experiments and air quality studies.

2 Methods

2.1 ICOIN-RACM2 Description

The ICOIN-RACM2 mechanism was based on the widely used RACM2 gas-phase chemical mechanism framework (Goliff et al., 2013). The RACM2 mechanism was developed to be able to simulate remote to polluted conditions from the surface to the upper troposphere. The mechanism includes 46 reactions to represent inorganic chemistry. The mechanism aggregates organic reactions based on the magnitude of emission rates, similarities in functional groups, and the compounds' reactivity (Stockwell et al., 1997) and consists of 54 stable organic species, 42 organic intermediates, 317 reactions, including 24 photolysis reactions. Overall, the RACM2 simulated concentrations of gas-phase products compare favorably to environmental chamber data (Goliff et al., 2013).

To simulate $\Delta(^{17}O)$ in various NO_y and O_x molecules, the transfer and propagation of O atoms deriving from O_3 were explicitly modeled in the employed chemical mechanism. Previously, a study developed a kinetic model that explicitly tracks the ^{16}O, ^{17}O, and ^{18}O abundance involving $NO_x/O_3/O_2$ reactions (Michalski et al., 2014). Here, we have adapted and simplified this

https://doi.org/10.5194/egusphere-2023-2293
Preprint. Discussion started: 26 October 2023

Table 1. Summary of the major formation pathways of several NO_y components, reaction types, and their expected $\Delta(^{17}O)$ values based on oxygen isotope mass-balance. X refers to halogens (Br, Cl, and I) and HC refers to hydrocarbons.

Formation Pathway	Type	$\Delta(^{17}O))/‰)$
	NO_2	
$NO + O_3$	Homogeneous	$\frac{1}{2}$ ($\Delta(^{17}O, NO)$) + $\frac{1}{2}$ ($\Delta(^{17}O, O_3{}^{term})$)
$NO + RO_2$	Homogeneous	$\frac{1}{2}$ ($\Delta(^{17}O, NO)$) + $\frac{1}{2}$ ($\Delta(^{17}O, RO_2)$)
$NO + HO_2$	Homogeneous	$\frac{1}{2}$ ($\Delta(^{17}O, NO)$) + $\frac{1}{2}$ ($\Delta(^{17}O, HO_2)$)
NO + XO	Homogeneous	$\frac{1}{2}$ ($\Delta(^{17}O, NO)$) + $\frac{1}{2}$ ($\Delta(^{17}O, XO)$)
	HONO	
NO + OH	Homogeneous	$\frac{1}{2}$ ($\Delta(^{17}O, NO)$) + $\frac{1}{2}$ ($\Delta(^{17}O, OH)$)
$NO_2 + H_2O_{(aq)}$	Heterogeneous	$\Delta(^{17}O, NO_2)$
	RO_2NO_2[*]	
$NO_2 + RO_2$	Homogeneous	$\frac{2}{3}$ ($\Delta(^{17}O, NO_2)$) + $\frac{1}{3}$ ($\Delta(^{17}O, RO_2)$)
	$RONO_2$[*]	
$NO + RO_2$	Homogeneous	$\frac{1}{3}$ ($\Delta(^{17}O, NO)$) + $\frac{2}{3}$ ($\Delta(^{17}O, RO_2)$)
$NO_3 + HC$	Homogeneous	$\Delta(^{17}O, NO_3)$
	HNO_3	
$NO_2 + OH$	Homogeneous	$\frac{2}{3}$ ($\Delta(^{17}O, NO_2)$) + $\frac{1}{3}$ ($\Delta(^{17}O, OH)$)
$NO_3 + HC$	Homogeneous	($\Delta(^{17}O, NO_3)$)
$NO + HO_2$	Homogeneous	$\frac{1}{3}$ ($\Delta(^{17}O, NO)$) + $\frac{2}{3}$ ($\Delta(^{17}O, HO_2)$)
$N_2O_5 + H_2O_{(aq)}$	Heterogeneous	$\frac{5}{6}$ ($\Delta(^{17}O, N_2O_5)$) + $\frac{1}{6}$ ($\Delta(^{17}O, H_2O)$)
$XNO_3 + H_2O_{(aq)}$	Heterogeneous	($\Delta(^{17}O, XNO_3)$)
$NO_2 + H_2O_{(aq)}$	Heterogeneous	$\frac{2}{3}$ ($\Delta(^{17}O, NO_2)$) + $\frac{1}{3}$ ($\Delta(^{17}O, H_2O)$)
$NO_3 + H_2O_{(aq)}$	Heterogeneous	($\Delta(^{17}O, NO_3)$)
$RONO_2 + H_2O_{(aq)}$	Heterogeneous	($\Delta(^{17}O, RONO_2)$)

[a] $\Delta(^{17}O)$ calculated from the nitrooxy ($-NO_3$) functional group

https://doi.org/10.5194/egusphere-2023-2293
Preprint. Discussion started: 26 October 2023

model to explicitly track the transfer and propagation of O atoms derived from the terminal end of O_3 without simulating and tracking the absolute ^{16}O, ^{17}O, and ^{18}O abundances, which can be tedious to employ in a detailed chemical mechanism. Our approach tagged O atoms transferred from O_3 as "Q" and tracking the interactions and propagation of "Q" among NO_y and O_x isotopologues using mass-balance and considering isotopologue reaction stoichiometry. The tagging of O isotopologues was not conducted for large O-reservoirs, including O_2 and H_2O. The reaction mechanism involved reactions with a single tagged O isotopologue, in which one tagged O isotopologue compound was found in the reactant and product, for example, NO + O_3 → NOQ + O_2 and NQ + O_3 → NQ_2 + O_2. Additionally, the mechanism involved reactions containing multiple tagged O compounds in the reactants and products, for example, NQ + NO_3 → NOQ + NO_2. For these multiple O-tagged isotopologue reactions, statistical probabilities, and mass-balance was considered in the product distributions. The explicit tracking and propagation of "Q" in the ICOIN-RACM2 lead to the rename of 19 reactions, the addition of 727 reactions replicated for the considered O isotopologues, and the addition of 55 oxygen isotopologues of NO_y and O_x relative to RACM2. Additionally, 26 oxygen isotope exchange reactions were added to the ICOIN-RACM2 chemical mechanism (Lyons, 2001) (Table 2).

Based on the model output of the concentrations of the oxygen isotopologues, the $\Delta(^{17}O)$ of various NO_y and HO_x molecules were calculated, as the following (Eq. 1):

$$\Delta(^{17}O, X) = f(Q) \times \Delta(^{17}O, O_3{}^{term}) \quad (1)$$

where X refers to the various NO_y and O_x molecules and f(Q) is the fractional amount of O-atoms deriving from O_3 for a particular molecule (i.e., the fractional amount of "Q"-atoms). The $\Delta(^{17}O, O_3{}^{term})$ represents the $\Delta(^{17}O)$ value of the terminal and transferable O atom of O_3. This value was assumed to be (39.3 ± 2.0 ‰), based on surface-level collections of O_3 on a nitrite coated filter (Vicars and Savarino, 2014). The f(Q) for the various considered molecules is calculated as followed (Eq. 2):

$$f(Q, X) = \frac{\sum_{i=1}^{j} i \cdot [Z_{\text{with iQ}}(X)]}{\sum_{i=0}^{j} j \cdot [Z(X)]} \quad (2)$$

where Z represents the oxygen isotopologues of molecule X, which can contain Q ($Z_{\text{with iQ}}$) or not, i represents the number of Q isotopes present in each Z of X, and j represents the maximum number of Q isotopes that can exist in X. Overall, this equation considers the distribution of Q isotopes within different arrangements and calculates the fraction of Q isotopes in the molecule relative to the total number of oxygen atoms.

We note that the RACM2 mechanism is a gas-phase mechanism and does not include heterogeneous reactions which could limit the ICOIN-RACM2 mechanism's ability to accurately simulate $\Delta(^{17}O)$ values, particularly of HONO and HNO_3 (Table 1). Gas-phase mechanisms are often used in larger chemical transport models that also include aerosol modules to calculate heterogeneous chemistry reaction rates. When utilizing ICOIN-RACM2 to simulate $\Delta(^{17}O)$ values (and RACM2 for simulating concentrations) in box models that lack aerosol modules, appropriate reactions should be included using pseduo-first-order

https://doi.org/10.5194/egusphere-2023-2293
Preprint. Discussion started: 26 October 2023

Table 2. Summary of the considered O exchange reactions, and reaction rates in the ICOIN-RACM2 mechanism. These reactions were adapted from Lyons (2001).

Label	Reaction	*k*
O-Exchange01	$Q(^3P) \xrightarrow{+O_2} O(^3P)$	$2.9\times10^{-12}[O_2]$ (s^{-1})
O-Exchange02	$Q(^1D) \xrightarrow{+O_2} O(^1D)$	$2.9\times10^{-12}[O_2]$ (s^{-1})
O-Exchange03	$Q(^1D) + NO \rightarrow O(^1D) + NQ$	3.7×10^{-11} (cm^3 $molecule^{-1}$ s^{-1})
O-Exchange04	$O(^1D) + NQ \rightarrow Q(^1D) + NO$	3.7×10^{-11} (cm^3 $molecule^{-1}$ s^{-1})
O-Exchange05	$Q(^3P) + NO \rightarrow O(^3P) + NQ$	3.7×10^{-11} (cm^3 $molecule^{-1}$ s^{-1})
O-Exchange06	$O(^3P) + NQ \rightarrow Q(^3P) + NO$	3.7×10^{-11} (cm^3 $molecule^{-1}$ s^{-1})
O-Exchange07	$QH \xrightarrow{+H_2O} OH$	$2.3\times10^{-13}e^{(-2100/T(K))}[H_2O]$ (s^{-1})
O-Exchange08	$QH \xrightarrow{+O_2} OH$	$1.0\times10^{-17}[O_2]$ (s^{-1})
O-Exchange09	$QH + HO_2 \rightarrow OH + HOQ$	$1.0\times10^{-11}e^{(400/T(K))}$ (cm^3 $molecule^{-1}$ s^{-1})
O-Exchange10	$OH + HOQ \rightarrow 0.5QH + 0.5HO_2 + 0.5OH + 0.5HOQ$	$1.0\times10^{-11}e^{(400/T(K))}$ (cm^3 $molecule^{-1}$ s^{-1})
O-Exchange11	$QH + HOQ \rightarrow 0.5OH + 0.5HQ_2 + 0.5QH + 0.5HOQ$	$1.0\times10^{-11}e^{(400/T(K))}$ (cm^3 $molecule^{-1}$ s^{-1})
O-Exchange12	$OH + HQ_2 \rightarrow QH + HOQ$	$1.0\times10^{-11}e^{(400/T(K))}$ (cm^3 $molecule^{-1}$ s^{-1})
O-Exchange13	$HOQ \xrightarrow{+O_2} HO_2$	$3.0\times10^{-17}[O_2]$ (s^{-1})
O-Exchange14	$HQ_2 \xrightarrow{+O_2} HO_2$	$3.0\times10^{-17}[O_2]$ (s^{-1})
O-Exchange15	$NQ + NO_2 \rightarrow NO + NOQ$	3.6×10^{-14} (cm^3 $molecule^{-1}$ s^{-1})
O-Exchange16	$NO + NOQ \rightarrow 0.5NQ + 0.5NO_2 + 0.5NO + 0.5NOQ$	3.6×10^{-14} (cm^3 $molecule^{-1}$ s^{-1})
O-Exchange17	$NQ + NOQ \rightarrow 0.5NO + 0.5NQ_2 + 0.5NQ + 0.5NOQ$	3.6×10^{-14} (cm^3 $molecule^{-1}$ s^{-1})
O-Exchange18	$NO + NQ_2 \rightarrow NQ + NOQ$	3.6×10^{-14} (cm^3 $molecule^{-1}$ s^{-1})
O-Exchange19	$NOQ \xrightarrow{+O_2} NO_2$	$1.0\times10^{-24}[O_2]$ (s^{-1})
O-Exchange20	$NQ_2 \xrightarrow{+O_2} NO_2$	$1.0\times10^{-24}[O_2]$ (s^{-1})
O-Exchange21	$QH + NO \rightarrow OH + NQ$	1.8×10^{-11} (cm^3 $molecule^{-1}$ s^{-1})
O-Exchange22	$OH + NQ \rightarrow QH + NO$	1.8×10^{-11} (cm^3 $molecule^{-1}$ s^{-1})
O-Exchange23	$QH + NO_2 \rightarrow OH + NOQ$	1.0×10^{-11} (cm^3 $molecule^{-1}$ s^{-1})
O-Exchange24	$OH + NOQ \rightarrow 0.5QH + 0.5NO_2 + 0.5OH + 0.5NOQ$	1.0×10^{-11} (cm^3 $molecule^{-1}$ s^{-1})
O-Exchange25	$QH + NOQ \rightarrow 0.5OH + 0.5NQ_2 + 0.5QH + 0.5NOQ$	1.0×10^{-11} (cm^3 $molecule^{-1}$ s^{-1})
O-Exchange26	$OH + NQ_2 \rightarrow QH + NOQ$	1.0×10^{-11} (cm^3 $molecule^{-1}$ s^{-1})

reaction rate constants to calculate heterogeneous hydrolysis. However, estimating the heterogeneous reaction rates is not trivial and depends on the molecular speed, and uptake coefficients which are dependent on aerosol chemical composition, and aerosol surface area density. These reaction rates may need to be treated in a case-by-case circumstance.

https://doi.org/10.5194/egusphere-2023-2293
Preprint. Discussion started: 26 October 2023

2.2 Box Model Description

The ICOIN-RACM2 mechanism was utilized in the Framework for 0-D Atmospheric Modeling (F0AM) box-model (Wolfe et al., 2016). This box model presents a high degree of flexibility, allowing it to be seamlessly adapted for a wide range of simulation scenarios, and can perform online computation of photolysis frequencies. The ICOIN-RACM2 mechanism was developed for use in the F0AM. In this work, the F0AM model was utilized to illustrate the capacity of the ICOIN-RACM2 mechanism for simulating $\Delta(^{17}O)$ values from photochemical chamber experiments and steady-state diel cycles.

2.2.1 Chamber Simulations

Box model simulations were conducted to evaluate α-pinene and NO_x chemistry under various initial conditions that included variable [α-pinene]:[NO_x] ratios (Table 3). These simulations were conducted using similar initial VOC and H_2O_2 levels utilized in recently conducted chamber experiments (Takeuchi and Ng, 2019). We have also varied the initial VOC and NO_x concentration levels to look at the impact on changing initial conditions and model chemistry on $\Delta^{17}O$ values. α-pinene is an important monoterpene, and its oxidation in the presence of NO_x constitutes an important mechanism of coupled biogenic-anthropogenic interaction, with important consequences for air quality, climate, global reactive nitrogen budget, and secondary organic aerosols (SOA) (Romer et al., 2016; Zare et al., 2018; Ng et al., 2017). The model was initiated for each experiment using NO, α-pinene, and H_2O_2 (OH precursor) concentrations. The α-pinene and H_2O_2 concentrations were fixed at 25 ppb and 2,000 ppb, respectively, while the initial NO concentrations were varied from 5 to 125 ppb to simulate oxidation chemistry in a range of [α-pinene]:[NO_x] conditions (Table 3). The pressure, temperature, and relative humidity were fixed at 1013 mbar, 295 K, and 1 %, respectively. The measured chamber light flux data from the Georgia Institute of Technology, Environmental Chamber Facility was also utilized.

The model was run for four hours for each simulated experiment. Both gas and particle chamber wall loss were not considered in the chamber simulation comparison. Monoterpene organic nitrate hydrolysis can be an important loss process and formation pathway of HNO_3 (Zare et al., 2018; Fisher et al., 2016; Takeuchi and Ng, 2019; Wang et al., 2021) but was not considered in the model because of the low relative humidity conditions. Additionally, heterogeneous pathways leading to the production of HNO_3, such as N_2O_5, were not included. For the hypothetical simulations, this should not impact the reliability of the predictions due to the photochemical conditions of the simulated chamber experiments, low relative humidity, and high organic carbon content of produced particles, which would be reasonably expected to lead to a low N_2O_5 uptake coefficient (Escorcia et al., 2010). When utilizing the ICOIN-RACM2 mechanism to simulate chamber experimental $\Delta(^{17}O)$ data, gas and particle wall-loss, organic nitrate hydrolysis, and NO_y heterogeneous reactions should be considered, but it will depend on the chamber and reaction conditions and should be treated in a case-by-case circumstance. The model simulations evaluated the $\Delta(^{17}O)$ temporal variation of NO_2, HONO, monoterpene-derived organic nitrate (ONIT), HNO_3, OH, and HO_2 and investigated their hypothetical changes in response to the experimental oxidant conditions.

https://doi.org/10.5194/egusphere-2023-2293
Preprint. Discussion started: 26 October 2023

Table 3. Summary of the precursor concentrations for the box-model simulations of α-pinene and NO photochemical oxidation chamber experiments. All experiments were simulated at a fixed temperature and relative humidity of 22 °C and 1 %, respectively.

Exp.	α-pinene/ppb	H_2O_2/ppb	NO/ppb	[α-pinene]:[NO]
1	25	2,000	5	5:1
2	25	2,000	10	2.5:1
3	25	2,000	25	1:1
4	25	2,000	62.5	1:2.5
5	25	2,000	125	1:5

2.2.2 Diel Variations

Box-model simulations were also conducted in steady-state diel cycles for two hypothetical summertime situations. These situations (Case 19 and Case 20) were based on previous case studies utilized to evaluate the RACM and RACM2 mechanism (Stockwell et al., 1997; Goliff et al., 2013). Briefly, Case 19 represents a somewhat polluted atmosphere with emissions of NO_x and organic compounds, and Case 20 represents a relatively cleaner atmosphere with the initial concentrations and emission rates of NO_x and organic compounds reduced by a factor of 10 (Table 4). These scenarios would be analogous to near-surface summertime environments. The box-model simulations were conducted for the initial conditions and with a fixed elevation of 0 km, temperature of 298 K, pressure of 1013.25 mbar, and for June 21 as previously described (Stockwell et al., 1997). The simulations were conducted for Providence, RI (41.82 °N, 71.41 °W) and the diel photolysis rates were calculated using the on-line module in F0AM (Wolfe et al., 2016). To avoid the buildup of concentrations in the box model, a dilution lifetime of 24 hours was incorporated into the simulations, as previously described (Wolfe et al., 2016). The model simulations were run for five days at a one-hour interval. The first two days of the simulation were used as a spin-up period and the diel cycles were evaluated from the average of the final three days of the simulation.

In order to more accurately predict ambient atmosphere $\Delta(^{17}O)$ values, additional NO_y heterogeneous reactions involving NO_2 and N_2O_5 were incorporated into the RACM2 mechanism and appropriately replicated for Q isotopes in the ICOIN-RACM2 mechanism (Table 5). The reaction rate for N_2O_5 was taken from the Master Chemical Mechanism (MCM) version 3.3.1 estimate for a general ambient air scenario. The NO_2 heterogeneous reaction rate was then scaled based on the relative ratio of their uptake coefficients to N_2O_5 for an organic carbon aerosol with RH > 30 % (Holmes et al., 2019). While we do not claim these heterogeneous reaction rates are perfectly constrained nor could be generalized to other modeling scenarios, they are useful for the diel simulations to evaluate $\Delta(^{17}O)$ changes in daytime versus nighttime chemistry. The inclusion of the NO_2 and N_2O_5 heterogeneous reactions in the utilized gas-phase mechanisms were termed RACM2(het) and ICOIN-RACM2(het), respectively. We note that the inclusion of organic nitrate hydrolysis was not considered in the diel simulations.

https://doi.org/10.5194/egusphere-2023-2293
Preprint. Discussion started: 26 October 2023

This was because conditions for Case 19 and Case 20 did not include either an initial concentration or emission rate for BVOC compounds (Table 4).

3 Results and Discussion

3.1 Mechanism Evaluation

The efficacy of the isotope tagging methodology was assessed through a comparative analysis of molecule concentrations using both the RACM2 and ICOIN-RACM2 mechanisms. For molecules encompassing oxygen isotopologues explicitly considered in the ICOIN-RACM2 mechanism, the concentrations were derived by summing the isotopologue concentrations (Eq. 3).

$$[X] = \sum_i [Z]_i \tag{3}$$

where [X] refers to the concentration of a molecule with oxygen isotopologues, i refers to the unique oxygen isotopologues, and [Z_i] refers to the concentration of the ith isotopologue. Both the RACM2 and ICOIN-RACM2 mechanisms simulated identical concentrations across both simulated scenarios: the hypothetical chamber experiments and the diurnal variation case study during the summer period (Fig. 1). This congruence in results aligns with expectations, as the isotope tagging approach implemented in the ICOIN-RACM2 is designed not to alter the chemical kinetics governing gas-phase reactions. Indeed, by definition, the presence of isotopes should remain inert with regard to chemical reactivity. This comparative analysis serves as a robust validation of the isotope tagging methodology's ability in simulating $\Delta(^{17}O)$ values while maintaining the chemical reactivity stipulated by the RACM2 mechanism.

3.2 Chamber Simulations of NO_x/α-pinene Chemistry

The simulated $\Delta(^{17}O)$ values derived from the hypothetical chamber simulations reveal significant temporal variations (Fig. 2). Overall, there were significant differences in $\Delta(^{17}O)$ values across the considered molecules that increased in the sequence of HO_2, OH, ONIT, HNO_3, HONO, and NO_2. Among the considered NO_y molecules, the initial $\Delta(^{17}O)$ values start at 0 ‰ and subsequently rises due to the generation of O_3 and subsequent propagation into the NO_y components, which leads to heightened $\Delta(^{17}O)$ values. The extent of $\Delta(^{17}O)$ elevation was determined to be contingent upon the initial chamber conditions, becoming more pronounced with increasing initial NO to α-pinene ratios for $\Delta(^{17}O, NO_2, HONO, HNO_3)$. An intriguing observation was that the simulated $\Delta(^{17}O, ONIT)$ values remained unaffected by the chamber's initial conditions. This observation underscores the diverse ONIT formation pathways present in the experiments, encompassing a $\Delta(^{17}O, ONIT)$ low-end pathway involving α-pinene peroxy radical (APIP; a type of RO_2) + NO, and a high-end pathway involving nitrooxy peroxy (nRO_2) deriving from α-pinene + NO_3 reactions (Table 1). We note that even though all of the simulated experiments were conducted under photochemical conditions, the model predicted some oxidation of α-pinene with NO_3. The relative proportion of these two significant ONIT formation routes exhibited substantial variability across the various experiments (Fig. 3). Generally, a higher

https://doi.org/10.5194/egusphere-2023-2293
Preprint. Discussion started: 26 October 2023

Table 4. Conditions for the box-model simulations of the diel cycle for two summertime scenarios. The simulations were conducted at a fixed elevation of 0 km, temperature of 298 K, pressure of 1013.25 mbar, and on June 21, 2015, in Providence, RI (41.82 °N, 71.41 °W). The scenarios were adapted from Stockwell et al. (1997).

	Case 19		Case 20	
Compound	Initial Conc/(ppb)	Emission Rate/(ppt/hr)	Initial Conc/(ppb)	Emission Rate/(ppt/hr)
		Inorganics		
NO	0.2	2.6	0.02	0.26
NO_2	0.5	—	0.05	—
HNO_3	0.1	—	0.01	—
O_3	50	—	30	—
H_2O_2	2.0	—	0.2	—
SO_2	—	0.52	—	0.052
CO	200	5.7	104	0.57
		Alkanes		
CH_4	1700	—	1700	—
ETH	—	0.24	—	0.024
HC3	—	2.6	—	0.26
HC5	—	0.76	—	0.076
HC8	—	0.45	—	0.045
		Alkenes		
ETE	—	0.46	—	0.046
OLI	—	0.19	—	0.019
OLT	—	0.22	—	0.022
		Aromatics		
TOL	—	0.57	—	0.057
XYL	—	0.52	—	0.052
		Carbonyls		
HCHO	1.0	0.14	0.1	0.014
ALD	—	0.036	—	0.0036
KET	—	0.32	—	0.032

https://doi.org/10.5194/egusphere-2023-2293
Preprint. Discussion started: 26 October 2023

Table 5. Summary of the NO_y heterogeneous reactions, assumed uptake coefficients, and the reference or calculated pseudo-first order reaction rates adapted in the RACM2(het) and ICOIN-RACM2(het) chemical mechanisms.

Label	Reaction	γ^a	$k_{het}(s^{-1})$
Het01	$NO_2 \rightarrow 0.5HNO_3 + 0.5HONO$	(10^{-6})	$(2.67\times10^{-6})^b$
Het02	$N_2O_5 \rightarrow 2HNO_3$	(1.5×10^{-4})	$(4.0\times10^{-4})^c$

[a] Adapted from Holmes et al. (2019)

[b] Calculated by scaling the k_{het} (N_2O_5) based on the relative γ

[c] Taken from the MCM v3.3.1 for general ambient scenarios.

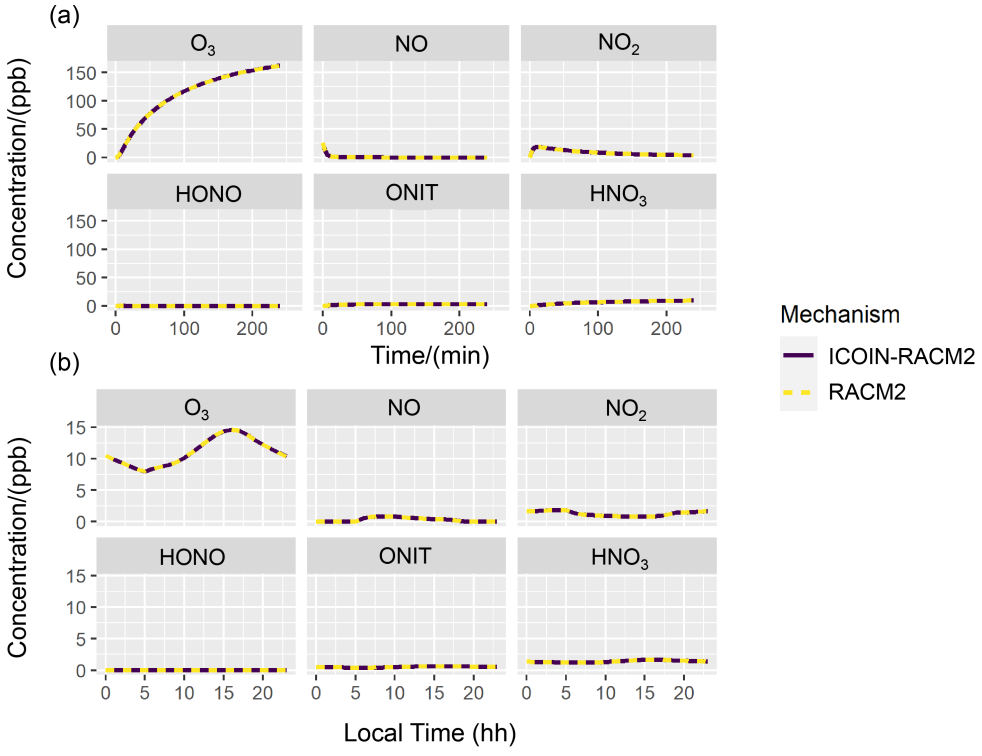

Figure 1. Comparison of the RACM2 (dashed yellow line) and ICOIN-RACM2 (purple solid line) mechanisms for simulating concentrations of several molecules for (a) Chamber Experiment-3 and (b) Diel Cycle-Case 19.

fractional formation of ONIT occurred through the $\Delta(^{17}O)$ high-end member pathway of nRO_2 + Y (where Y = HO_2, NO, nRO_2, ACO_3, MO_2) as the initial NO to α-pinene ratios were lower. Additionally, we note that the produced $\Delta(^{17}O$, ONIT) value is a balance between the ONIT production pathway and the $\Delta(^{17}O$, NO) (Table 1). For the lower initial [NO_x]:[α-pinene] experiments, a lower $\Delta(^{17}O$,NO) value was simulated. The balance between $\Delta(^{17}O$, NO) and the pathway leading to ONIT production can explain the observation that $\Delta(^{17}O$, ONIT) was insensitive to initial conditions.

https://doi.org/10.5194/egusphere-2023-2293
Preprint. Discussion started: 26 October 2023

In contrast, $\Delta(^{17}O, HO_2)$ was nearly negligible, aligning with common assumptions in other $\Delta(^{17}O)$ models (Alexander et al., 2019, 2009; Michalski et al., 2003; Morin et al., 2011). Similarly, $\Delta(^{17}O, OH)$ generally maintained close proximity to 0 ‰, in line with typical assumptions in other $\Delta(^{17}O)$ models (Alexander et al., 2019, 2009; Michalski et al., 2003; Morin et al., 2011); although there were instances that deviated from this trend. Notably, higher $\Delta(^{17}O, OH)$ values were observed as the initial NO_x relative to BVOC concentrations increased. This occurrence can be attributed to the increased significance of oxygen isotope exchange between NO_2 and OH for the higher initial NO_x experimental conditions.

The simulated $\Delta(^{17}O)$ values from the chamber experiments highlight compelling dynamics. Primarily, there were substantial differences in $\Delta(^{17}O)$ values arising from different formation pathways contributing to ONIT production. The uncertain nature of branching ratios and product yields for ONIT underscores the potential utility of comparing $\Delta(^{17}O, ONIT)$ observations with model simulations, aiding in the refinement of our understanding of ONIT yields originating from APIP + NO and API + NO_3 reaction pathways. Furthermore, a significant divergence between HNO_3 and ONIT in terms of $\Delta(^{17}O)$ was observed, particularly with heightened initial NO to α-pinene concentrations. This divergence led to considerably higher simulated $\Delta(^{17}O, HNO_3)$ than $\Delta(^{17}O, ONIT)$. This difference could potentially be utilized to help constrain the contribution of ONIT hydrolysis to HNO_3 through a comparison of observed $\Delta(^{17}O, HNO_3)$ and model-based predictions. Lastly, the model simulations underscore the potential of employing the ICOIN-RACM2 model to corroborate $\Delta(^{17}O)$ values for OH and HO_2 under diverse conditions (such as concentrations, chemical composition, relative humidity, and temperature), which are commonly assumed to be 0 ‰.

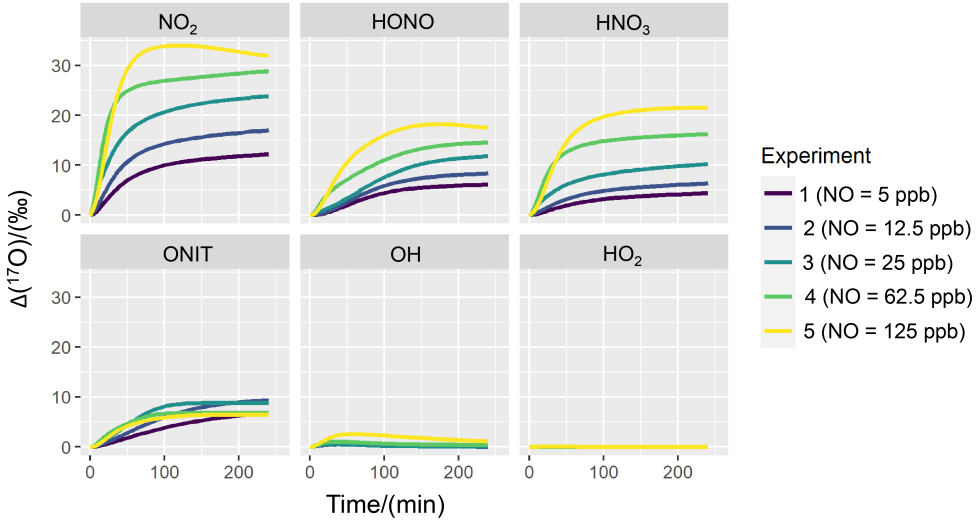

Figure 2. Simulation of $\Delta(^{17}O)$ for several NO_y and O_x molecules including, NO_2, HONO, HNO_3, ONIT, OH, and HO_2 for the various hypothetical chamber experiments (color-coded).

https://doi.org/10.5194/egusphere-2023-2293
Preprint. Discussion started: 26 October 2023

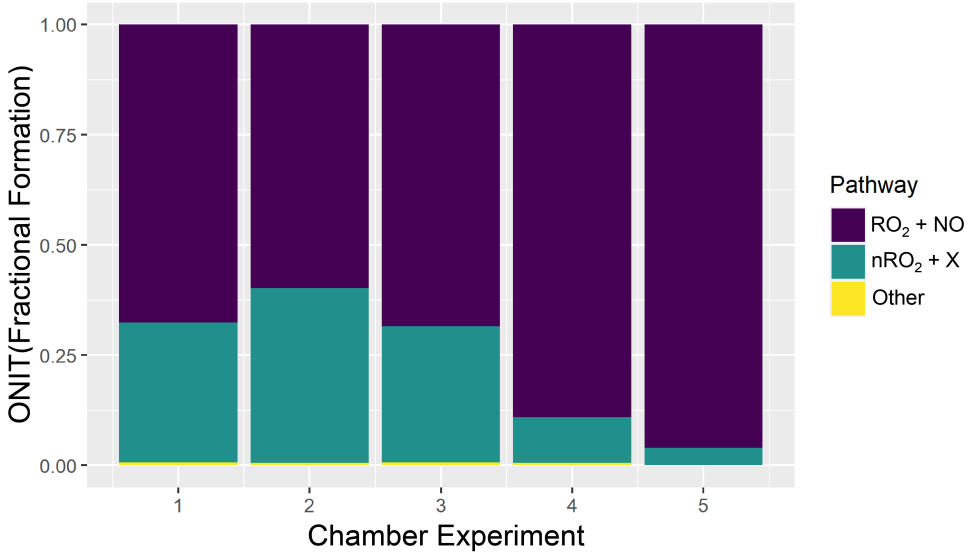

Figure 3. Simulation of ONIT fractional formation pathways for the various hypothetical chamber experiments.

3.3 Summertime Diel Simulations

The simulated $\Delta(^{17}O)$ diel profiles indicate interesting patterns for the various considered molecules, including NO, NO_2, HONO, HNO_3, OH, and HO_2 (Fig. 4). The $\Delta(^{17}O, NO, NO_2, HONO)$ indicates a strong diurnal pattern for both considered summertime case studies. The simulated $\Delta(^{17}O, NO, NO_2)$ indicates lower values during the nighttime and higher values during the daytime. This is due to the importance of nighttime NO emissions, such that the O atoms of NO and NO_2 are not photochemically cycled and there are significant O-atom contributions from NO emission sources in the nighttime $\Delta(^{17}O, NO, NO_2)$, perturbing NO_x from a photochemical steady state as commonly assumed in previous $\Delta(^{17}O)$ models. Still, the nighttime $\Delta(^{17}O, NO)$ does not reach 0 ‰, due to the presence of some daytime NO that has been photochemically cycled. These diel cycles are consistent with summertime $\delta(^{18}O, NO_2)$ observations (which track with $\Delta(^{17}O, NO_2)$) in West Lafayette, IN, US (Walters et al., 2018), and recent diel observations of $\Delta(^{17}O, NO_2)$ at Grenoble, FR, during the spring (Albertin et al., 2021).

The simulated daytime profiles of $\Delta(^{17}O, NO, NO_2)$ follow similar patterns, reflecting their fast photochemical cycling. Near sunrise, $\Delta(^{17}O, NO, NO_2)$ reaches a peak due to photochemical cycling that primarily involves O_3. As photolysis continues, there is a significant enhancement of peroxy radicals (RO_2/HO_2), which slightly dilutes the $\Delta(^{17}O, NO, NO_2)$. Near sunset, the peroxy radical concentrations decrease, and once again NO and NO_2 predominantely photochemically cycle with O_3.

The diurnal variation in $\Delta(^{17}O, HONO)$ exhibits an inverse pattern compared to NO and NO_2, characterized by nocturnal maxima and daytime minima. This contrast arises from distinct formation pathways operating during daytime and nighttime. HONO formation predominantly occurs via NO_2 heterogeneous reactions during the night, giving rise to a high-$\Delta(^{17}O, HONO)$ end-member (Table 1). Conversely, daytime HONO production centers around the NO + OH pathway, leading to a low-$\Delta(^{17}O,$

https://doi.org/10.5194/egusphere-2023-2293
Preprint. Discussion started: 26 October 2023

HONO) end-member, assuming $\Delta(^{17}O, OH)$ is near 0 ‰, which dilutes the $\Delta(^{17}O)$ of the formed HONO relative to $\Delta(^{17}O,$ HONO, NO) (Table 1). Notably, primary emissions could significantly contribute to HONO levels but were excluded from the hypothetical summertime scenarios (Stockwell et al., 1997). If primary HONO emissions were substantial, a lower $\Delta(^{17}O,$ HONO) during the night would be anticipated due to a lack of NO_y photochemical cycling, assuming primary emissions carry a $\Delta(^{17}O, HONO)$ value of 0 ‰.

The $\Delta(^{17}O, HNO_3, OH, HO_2)$ had little variation in their diel profiles. The $\Delta(^{17}O, HNO_3)$ tended to converge to a value dependent on the oxidant conditions for Case 19 and Case 20. There were no significant simulated $\Delta(^{17}O, HNO_3)$ diurnal variability due to the relatively longer HNO_3 lifetime in the gas-phases mechanism relative to NO, NO_2, and HONO, which rapidly undergo photochemical cycling. In the RACM2 mechanism, the significant chemical loss pathways for HNO_3 are HNO_3 + OH and HNO_3 photolysis, which are relatively slow loss pathways, essentially "locking-in" the $\Delta(^{17}O, HNO_3)$ values. Thus, due to the relatively elevated HNO_3 lifetime, the simulated $\Delta(^{17}O, HNO_3)$ builds up toward a steady-state value. The simulated $\Delta(^{17}O, OH, HO_2)$ was near 0 ‰ for the entire simulation, consistent with previous $\Delta(^{17}O)$ model expectations (Alexander et al., 2019, 2009; Michalski et al., 2003; Morin et al., 2011).

Comparing Case 19 and Case 20 reveals coherent diel $\Delta(^{17}O)$ patterns. The primary disparity between these case studies lies in the higher $\Delta(^{17}O)$ values exhibited by the considered NO_y compounds in the urban setting of Case 19 compared to the rural backdrop of Case 20. This divergence in simulated $\Delta(^{17}O)$ stems from the interplay between O_3 and RO_2/HO_2. Urban conditions entail greater contributions from NO_x photochemical cycling with O_3 relative to the rural environment. These hypothetical simulations highlight the prospect of intriguing $\Delta(^{17}O)$ variations between urban and rural settings.

4 Conclusions

This study introduces a novel gas-phase mechanism, denoted as ICOIN-RACM2, which is built upon the RACM2 gas-phase chemical mechanism framework (Goliff et al., 2013). This mechanism is designed to explicitly model the $\Delta(^{17}O)$ isotopic composition within NO_y and O_x molecules based on quantitatively tracking the incorporation and propagation of O-atoms derived from O_3. Its application is demonstrated through box-model simulations encompassing diverse hypothetical scenarios. These scenarios include chamber experiments focused on α-pinene and NO photochemical oxidation, as well as the exploration of diurnal cycles in summertime chemistry.

These initial investigations serve as a fundamental step towards advancing our comprehension of NO_y oxidation chemistry and its intricate pathways. Notably, the mechanism exhibits promising capabilities in simulating $\Delta(^{17}O)$ values for multiple NO_y and O_x species. This capacity holds considerable promise for refining our insights into aspects such as ONIT formation, branching ratios, and hydrolysis dynamics. Moreover, the ICOIN-RACM2 mechanism emerges as a valuable tool for various air-quality-related objectives. It could be an invaluable tool for the assessment of primary emission strengths for HONO and the probing of urban-to-rural gradients of atmospheric oxidation chemistry. In forthcoming endeavors, this newly devised model

https://doi.org/10.5194/egusphere-2023-2293
Preprint. Discussion started: 26 October 2023

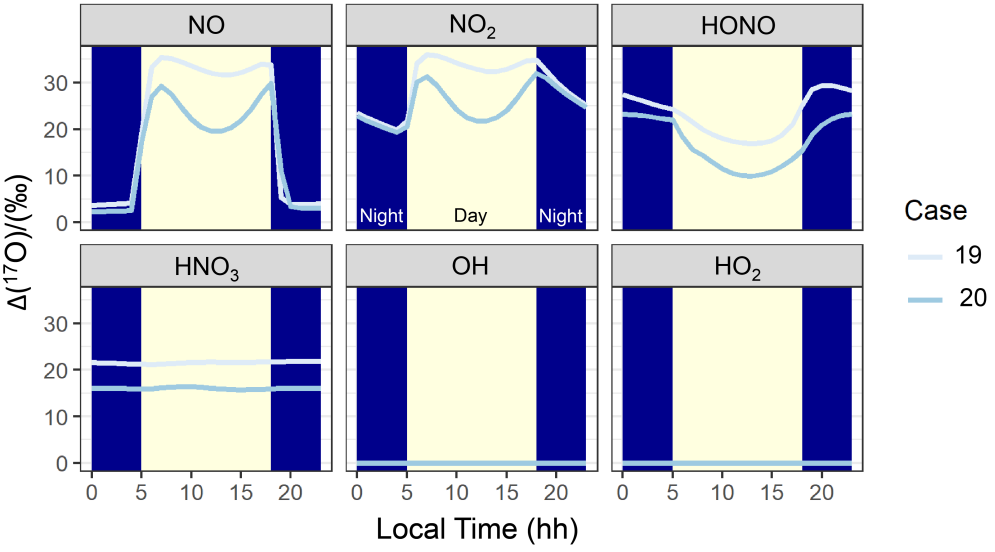

Figure 4. Diel simulation of $\Delta(^{17}O)$ for several NO_y and O_x molecules including, NO, NO_2, HONO, HNO_3, OH, and HO_2 for the various hypothetical summertime cases (color-coded). The shading corresponds to daytime (light yellow) and nighttime (dark blue) conditions.

will be instrumental in direct comparisons with $\Delta(^{17}O)$ observations arising from chamber experiments and investigations tied to air quality. As techniques for analyzing $\Delta(^{17}O)$ in NO_y molecules continue to advance, the model's utility is poised to expand.

An envisioned next step involves integrating the model into a broader 3-D atmospheric chemistry framework. This integration is anticipated to offer vital insights for evaluating the representation of oxidation chemistry across diverse landscapes. These endeavors have far-reaching implications, notably in fine-tuning our capacity to accurately model and predict atmospheric oxidation processes, thus enhancing our overall understanding of atmospheric oxidation capacity.

Code availability. The developed mechanism and box-model simulation input files are made available on GitHub (Walters, 2023)

.

Author contributions. WWW designed, tested, and evaluate the newly developed mechanism. MT and NLN provided critical insight into utilizing box-models to simulate chamber experimental data. WWW and MGH secured funding for this work. WWW prepared the article with contributions from all co-authors.

https://doi.org/10.5194/egusphere-2023-2293
Preprint. Discussion started: 26 October 2023

Competing interests. The contact author has declared that none of the authors have any competing interests.

https://doi.org/10.5194/egusphere-2023-2293
Preprint. Discussion started: 26 October 2023

References

Albertin, S., Savarino, J., Bekki, S., Barbero, A., and Caillon, N.: Measurement report: Nitrogen isotopes (δ^{15}N) and first quantification of oxygen isotope anomalies (Δ^{17}O, δ^{18}O) in atmospheric nitrogen dioxide, Atmospheric Chemistry and Physics, 21, 10 477–10 497, https://doi.org/10.5194/acp-21-10477-2021, publisher: Copernicus GmbH, 2021.

Alexander, B., Hastings, M. G., Allman, D. J., Dachs, J., Thornton, J. A., and Kunasek, S. A.: Quantifying atmospheric nitrate formation pathways based on a global model of the oxygen isotopic composition (Δ17O) of atmospheric nitrate, Atmos. Chem. Phys., 9, 5043–5056, https://doi.org/10.5194/acp-9-5043-2009, 2009.

Alexander, B., Sherwen, T., Holmes, C. D., Fisher, J. A., Chen, Q., Evans, M. J., and Kasibhatla, P.: Global inorganic nitrate production mechanisms: Comparison of a global model with nitrate isotope observations, Atmospheric Chemistry and Physics Discussions, pp. 1–36, https://doi.org/https://doi.org/10.5194/acp-2019-422, 2019.

Barkan, E. and Luz, B.: High-precision measurements of 17O/16O and 18O/16O of O2 and O2/Ar ratio in air, Rapid Communications in Mass Spectrometry, 17, 2809–2814, https://doi.org/10.1002/rcm.1267, 2003.

Blum, D. E., Walters, W. W., and Hastings, M. G.: Speciated Collection of Nitric Acid and Fine Particulate Nitrate for Nitrogen and Oxygen Stable Isotope Determination, Analytical Chemistry, 92, 16 079–16 088, publisher: ACS Publications, 2020.

Blum, D. E., Walters, W. W., Eris, G., Takeuchi, M., Huey, L. G., Tanner, D., Xu, W., Rivera-Rios, J. C., Liu, F., Ng, N. L., and Hastings, M. G.: Collection of Nitrogen Dioxide for Nitrogen and Oxygen Isotope DeterminationLaboratory and Environmental Chamber Evaluation, Analytical Chemistry, 95, 3371–3378, https://doi.org/10.1021/acs.analchem.2c04672, publisher: American Chemical Society, 2023.

Browne, E. C. and Cohen, R. C.: Effects of biogenic nitrate chemistry on the NO_x lifetime in remote continental regions, Atmospheric Chemistry and Physics, 12, 11 917–11 932, https://doi.org/10.5194/acp-12-11917-2012, publisher: Copernicus GmbH, 2012.

Chai, J. and Hastings, M. G.: Collection Method for Isotopic Analysis of Gaseous Nitrous Acid, Analytical Chemistry, 90, 830–838, https://doi.org/10.1021/acs.analchem.7b03561, 2018.

Escorcia, E. N., Sjostedt, S. J., and Abbatt, J. P. D.: Kinetics of N2O5 Hydrolysis on Secondary Organic Aerosol and Mixed Ammonium Bisulfate-Secondary Organic Aerosol Particles, The Journal of Physical Chemistry A, 114, 13 113–13 121, https://doi.org/10.1021/jp107721v, publisher: American Chemical Society, 2010.

Fisher, J. A., Jacob, D. J., Travis, K. R., Kim, P. S., Marais, E. A., Chan Miller, C., Yu, K., Zhu, L., Yantosca, R. M., Sulprizio, M. P., Mao, J., Wennberg, P. O., Crounse, J. D., Teng, A. P., Nguyen, T. B., Clair, J. M. S., Cohen, R. C., Romer, P., Nault, B. A., Wooldridge, P. J., Jimenez, J. L., Campuzano-Jost, P., Day, D. A., Hu, W., Shepson, P. B., Xiong, F., Blake, D. R., Goldstein, A. H., Misztal, P. K., Hanisco, T. F., Wolfe, G. M., Ryerson, T. B., Wisthaler, A., and Mikoviny, T.: Organic nitrate chemistry and its implications for nitrogen budgets in an isoprene- and monoterpene-rich atmosphere: constraints from aircraft (SEAC^{4}RS) and ground-based (SOAS) observations in the Southeast US, Atmospheric Chemistry and Physics, 16, 5969–5991, https://doi.org/https://doi.org/10.5194/acp-16-5969-2016, 2016.

Galloway, J. N., Dentener, F. J., Capone, D. G., Boyer, E. W., Howarth, R. W., Seitzinger, S. P., Asner, G. P., Cleveland, C. C., Green, P. A., Holland, E. A., Karl, D. M., Michaels, A. F., Porter, J. H., Townsend, A. R., and Vöosmarty, C. J.: Nitrogen Cycles: Past, Present, and Future, Biogeochemistry, 70, 153–226, https://doi.org/10.1007/s10533-004-0370-0, 2004.

Gao, Y. Q. and Marcus, R. A.: Strange and unconventional isotope effects in ozone formation, Science (New York, N.Y.), 293, 259–263, https://doi.org/10.1126/science.1058528, 2001.

https://doi.org/10.5194/egusphere-2023-2293
Preprint. Discussion started: 26 October 2023

Gen, M., Liang, Z., Zhang, R., Mabato, B. R. G., and Chan, C. K.: Particulate nitrate photolysis in the atmosphere, Environmental Science: Atmospheres, 2, 111–127, 2022.

Goliff, W. S., Stockwell, W. R., and Lawson, C. V.: The regional atmospheric chemistry mechanism, version 2, Atmospheric Environment, 68, 174–185, https://doi.org/10.1016/j.atmosenv.2012.11.038, 2013.

Hastings, M. G., Sigman, D. M., and Lipschultz, F.: Isotopic evidence for source changes of nitrate in rain at Bermuda, Journal of Geophysical Research: Atmospheres, 108, http://onlinelibrary.wiley.com/doi/10.1029/2003JD003789/full, 2003.

Holmes, C. D., Bertram, T. H., Confer, K. L., Graham, K. A., Ronan, A. C., Wirks, C. K., and Shah, V.: The Role of Clouds in the Tropospheric NOx Cycle: A New Modeling Approach for Cloud Chemistry and Its Global Implications, Geophysical Research Letters, 46, 4980–4990, https://doi.org/10.1029/2019GL081990, _eprint: https://onlinelibrary.wiley.com/doi/pdf/10.1029/2019GL081990, 2019.

Johnston, J. C. and Thiemens, M. H.: The isotopic composition of tropospheric ozone in three environments, Journal of Geophysical Research: Atmospheres (1984–2012), 102, 25 395–25 404, http://onlinelibrary.wiley.com/doi/10.1029/97JD02075/full, 1997.

Kim, H., Walters, W. W., Bekker, C., Murray, L. T., and Hastings, M. G.: Nitrate chemistry in the northeast US – Part 2: Oxygen isotopes reveal differences in particulate and gas-phase formation, Atmospheric Chemistry and Physics, 23, 4203–4219, https://doi.org/10.5194/acp-23-4203-2023, publisher: Copernicus GmbH, 2023.

Lyons, J. R.: Transfer of mass-independent fractionation in ozone to other oxygen-containing radicals in the atmosphere, Geophysical Research Letters, 28, 3231–3234, http://onlinelibrary.wiley.com/doi/10.1029/2000GL012791/full, 2001.

Michalski, G., Scott, Z., Kabiling, M., and Thiemens, M. H.: First measurements and modeling of Δ17O in atmospheric nitrate, Geophysical Research Letters, 30, 2003.

Michalski, G., Bhattacharya, S. K., and Mase, D. F.: Oxygen isotope dynamics of atmospheric nitrate and its precursor molecules, in: Handbook of environmental isotope geochemistry, pp. 613–635, Springer, 2012.

Michalski, G., Bhattacharya, S. K., and Girsch, G.: NO x cycle and the tropospheric ozone isotope anomaly: an experimental investigation, Atmospheric Chemistry and Physics, 14, 4935–4953, http://www.atmos-chem-phys.net/14/4935/2014/, 2014.

Morin, S., Sander, R., and Savarino, J.: Simulation of the diurnal variations of the oxygen isotope anomaly (Δ 17 O) of reactive atmospheric species, Atmospheric Chemistry and Physics, 11, 3653–3671, 2011.

Newsome, B. and Evans, M.: Impact of uncertainties in inorganic chemical rate constants on tropospheric composition and ozone radiative forcing, Atmospheric Chemistry and Physics, 17, 14 333–14 352, https://doi.org/https://doi.org/10.5194/acp-17-14333-2017, 2017.

Ng, N. L., Brown, S. S., Archibald, A. T., Atlas, E., Cohen, R. C., Crowley, J. N., Day, D. A., Donahue, N. M., Fry, J. L., Fuchs, H., Griffin, R. J., Guzman, M. I., Herrmann, H., Hodzic, A., Iinuma, Y., Jimenez, J. L., Kiendler-Scharr, A., Lee, B. H., Luecken, D. J., Mao, J., McLaren, R., Mutzel, A., Osthoff, H. D., Ouyang, B., Picquet-Varrault, B., Platt, U., Pye, H. O. T., Rudich, Y., Schwantes, R. H., Shiraiwa, M., Stutz, J., Thornton, J. A., Tilgner, A., Williams, B. J., and Zaveri, R. A.: Nitrate radicals and biogenic volatile organic compounds: oxidation, mechanisms, and organic aerosol, Atmos. Chem. Phys., 17, 2103–2162, https://doi.org/10.5194/acp-17-2103-2017, 2017.

Pinder, R. W., Davidson, E. A., Goodale, C. L., Greaver, T. L., Herrick, J. D., and Liu, L.: Climate change impacts of US reactive nitrogen, Proceedings of the National Academy of Sciences, 109, 7671–7675, https://doi.org/10.1073/pnas.1114243109, publisher: National Academy of Sciences Section: Physical Sciences, 2012.

Prinn, R. G.: The cleansing capacity of the atmosphere, Annual Review of Environment and Resources, 28, 29–57, publisher: Annual Reviews 4139 El Camino Way, PO Box 10139, Palo Alto, CA 94303-0139, USA, 2003.

https://doi.org/10.5194/egusphere-2023-2293
Preprint. Discussion started: 26 October 2023

Romer, P. S., Duffey, K. C., Wooldridge, P. J., Allen, H. M., Ayres, B. R., Brown, S. S., Brune, W. H., Crounse, J. D., De Gouw, J., and Draper, D. C.: The lifetime of nitrogen oxides in an isoprene-dominated forest, Atmospheric Chemistry and Physics, 16, 7623–7637, publisher: European Geosciences Union, 2016.

Savarino, J., Bhattacharya, S., Morin, S., Baroni, M., and Doussin, J.-F.: The NO+ O3 reaction: A triple oxygen isotope perspective on the reaction dynamics and atmospheric implications for the transfer of the ozone isotope anomaly, The Journal of chemical physics, 128, 2008.

Stockwell, W. R., Kirchner, F., Kuhn, M., and Seefeld, S.: A new mechanism for regional atmospheric chemistry modeling, Journal of geophysical research: Atmospheres, 102, 25 847–25 879, http://onlinelibrary.wiley.com/doi/10.1029/97JD00849/full, 1997.

Takeuchi, M. and Ng, N. L.: Chemical composition and hydrolysis of organic nitrate aerosol formed from hydroxyl and nitrate radical oxidation of α-pinene and β-pinene, Atmospheric Chemistry and Physics, 19, 12 749–12 766, publisher: Copernicus GmbH, 2019.

Vicars, W. C. and Savarino, J.: Quantitative constraints on the 17 O-excess (Δ 17 O) signature of surface ozone: Ambient measurements from 50° N to 50° S using the nitrite-coated filter technique, Geochimica et Cosmochimica Acta, 135, 270–287, http://www.sciencedirect.com/science/article/pii/S0016703714001884, 2014.

Walters, W.: Walters-Research-Group/ICOIN_RACM2: ICOIN_RACM2, https://doi.org/10.5281/zenodo.8418755, 2023.

Walters, W. W., Fang, H., and Michalski, G.: Summertime diurnal variations in the isotopic composition of atmospheric nitrogen dioxide at a small midwestern United States city, Atmospheric Environment, 179, 1–11, https://doi.org/10.1016/j.atmosenv.2018.01.047, 2018.

Walters, W. W., Michalski, G., Böhlke, J. K., Alexander, B., Savarino, J., and Thiemens, M. H.: Assessing the Seasonal Dynamics of Nitrate and Sulfate Aerosols at the South Pole Utilizing Stable Isotopes, Journal of Geophysical Research: Atmospheres, 124, 8161–8177, https://doi.org/10.1029/2019JD030517, 2019.

Wang, Y., Piletic, I. R., Takeuchi, M., Xu, T., France, S., and Ng, N. L.: Synthesis and hydrolysis of atmospherically relevant monoterpene-derived organic nitrates, Environmental science & technology, 55, 14 595–14 606, 2021.

Wang, Y., Takeuchi, M., Wang, S., Nizkorodov, S. A., France, S., Eris, G., and Ng, N. L.: Photolysis of gas-phase atmospherically relevant monoterpene-derived organic nitrates, The Journal of Physical Chemistry A, 127, 987–999, 2023.

Wolfe, G. M., Marvin, M. R., Roberts, S. J., Travis, K. R., and Liao, J.: The Framework for 0-D Atmospheric Modeling (F0AM) v3.1, Geoscientific Model Development, 9, 3309–3319, https://doi.org/https://doi.org/10.5194/gmd-9-3309-2016, 2016.

Zare, A., Romer, P. S., Nguyen, T., Keutsch, F. N., Skog, K., and Cohen, R. C.: A comprehensive organic nitrate chemistry: insights into the lifetime of atmospheric organic nitrates, Atmospheric Chemistry and Physics, 18, 15 419–15 436, https://doi.org/10.5194/acp-18-15419-2018, publisher: Copernicus GmbH, 2018.